J. Fluid Mech. (1990), *vol.* 211, *pp.* 309–332
Printed in Great Britain

Velocity, scalar and transfer spectra in numerical turbulence

By ROBERT M. KERR

Geophysical Turbulence Program, National Center for Atmospheric Research, PO Box 3000, Boulder, CO 80307-3000, USA

(Received 1 July 1985 and in revised form 19 July 1989)

Velocity and passive-scalar spectra for turbulent fields generated by a forced three-dimensional simulation with 128^3 grid points and Taylor-microscale Reynolds numbers up to 83 are shown to have convective and diffusive spectral regimes. One- and three-dimensional spectra are compared with experiment and theory. If normalized by the Kolmogorov dissipation scales and scalar dissipation, velocity spectra and scalar spectra for given Prandtl numbers collapse to single curves in the dissipation regime with exponential tails. If multiplied by $k^{\frac{5}{3}}$ the velocity spectra show an anomalously high Kolmogorov constant that is consistent with low Reynolds number experiments. When normalized by the Batchelor scales, the scalar spectra show a universal dissipation regime that is independent of Prandtl numbers from 0.1 to 1.0. The time development of velocity spectra is illustrated by energy-transfer spectra in which distinct pulses propagate to high wavenumbers.

1. Introduction

The most common tools for describing isotropic, homogeneous turbulence are spectra. In particular, theoretical, experimental, and numerical investigations of the $k^{-\frac{5}{3}}$ inertial subrange of the kinetic-energy spectrum, based on the second similarity hypothesis of Kolmogorov (1941), have become a small industry. A similar hypothesis predicts that the variance spectrum of a passive scalar has an inertial subrange (Oboukov 1949; Corrsin 1951), where examples of passive scalars are temperature and salinity, if buoyancy is neglected, and chemical reactants. Experiments strongly support the existence of a $k^{-\frac{5}{3}}$ inertial subrange for both the kinetic-energy and scalar-variance spectra (see Champagne 1978 for the velocity; references for the scalar are in § 4).

But the inertial subrange is only one part of the spectra. There are dissipation regimes and for the passive scalar there is an inertial–diffusive regime associated with low Prandtl numbers (high scalar diffusivity) and a viscous–convective regime associated with high Prandtl numbers (low scalar diffusivity). While all of these regimes have been measured experimentally to varying degrees of reliability, direct numerical simulations of turbulence would seem to be an even better means of determining these spectra. Conditions can be carefully controlled and because entire fields are available, one- and three-dimensional spectra can both be determined and higher-order spectra that are inaccessible to experiments can be found. However, the simulations have generally been restricted by small meshes to very low Reynolds numbers and the evidence for inertial regimes is marginal (Brachet *et al.* 1983). A case in which a short inertial subrange is found is the forced spectral simulations of Kerr (1985*a*) with up to 128^3 mesh points and Taylor-microscale Reynolds numbers R_λ up

to 83. In this paper the numerical data base used by Kerr (1985*a*) is examined further. First, one- and three-dimensional velocity spectra are presented and comparisons with low Reynolds number experiments made to show that this simulation represents low Reynolds number turbulence, a conclusion supported by derivative statistics in Kerr (1985*a*). Then dissipation and scalar variance regimes that are difficult to measure experimentally are discussed and compared to theoretical spectra. Finally, kinetic-energy transfer spectra are used to discuss intermittency in Fourier space. Some comparisons between the theoretical regimes and simulations are made where the conditions required by the theoretical regimes are not fully met by the simulations in order to provide guidance for future numerical experiments.

The spectral regimes of the kinetic energy and scalar variance are found in wavenumber bands determined by the largest scales of turbulence L (equation (21*b*)) and three dissipation scales. These dissipation scales and the associated scaling laws for the spectral regime of the kinetic energy and scalar variance depend on the kinetic-energy dissipation rate

$$\epsilon = 2\nu e_{ij}^2 \sim -\frac{\mathrm{d}}{\mathrm{d}t}\langle E\rangle, \tag{1}$$

the scalar-variance dissipation rate

$$\chi = 2\kappa\theta_{,i}^2 \sim -\frac{\mathrm{d}}{\mathrm{d}t}\langle E_\theta\rangle, \tag{2}$$

the viscosity ν, and the Prandtl number, $\sigma = \nu/\kappa$, where $E = \frac{1}{2}\langle u_i u_i\rangle$ is the kinetic energy and $E_\theta = \langle\theta^2\rangle$ is the scalar variance. The dissipation wavenumbers and corresponding lengthscales are the Kolmogorov scale

$$k_\mathrm{K} = (\epsilon/\nu^3)^{\frac{1}{4}} = 1/\eta, \tag{3a}$$

the Batchelor scale

$$k_\mathrm{B} = (\epsilon/\nu\kappa^2)^{\frac{1}{4}} = k_\mathrm{K}\sigma^{\frac{1}{2}} = 1/\eta_\mathrm{B} \tag{3b}$$

and the Oboukov–Corrsin scale

$$k_\mathrm{oc} = (\epsilon/\kappa^3)^{\frac{1}{4}} = k_\mathrm{K}\sigma^{\frac{3}{4}} = 1/\eta_\mathrm{oc}. \tag{3c}$$

The Kolmogorov inertial subrange of the kinetic-energy spectrum

$$E(k) = \alpha\epsilon^{\frac{2}{3}}k^{-\frac{5}{3}} \tag{4}$$

is found experimentally between the turbulent scale L (equation (21)) and the Kolmogorov scale η in high Reynolds number incompressible fluids. The first Kolmogorov similarity hypothesis is obeyed when all velocity and length scales are determined by the energy dissipation ϵ and viscosity ν and for (4) to satisfy Kolmogorov scaling the dimensionless Kolmogorov constant α should be universal when high Reynolds number spectra are scaled by

$$(\epsilon\nu^5)^{\frac{1}{4}} \tag{5}$$

and the wavenumbers are scaled by η. The dissipation regime usually refers to $k > 0.2k_\mathrm{K}$ and while it will not obey (4), it should obey Kolmogorov scaling under (5). All the velocity spectra to be discussed are scaled in this manner to determine if they obey Kolmogorov scaling, even if they do not have an inertial subrange. Pao (1965) predicts a dissipation regime proportional to $\exp(-(a\eta k)^{\frac{4}{3}})$, but based on analyticity (Von Neumann 1949; Frisch & Morf 1981) and closure (Kraichnan 1959) it has been suggested that the dissipation regime should be closer to a simple exponential like $\exp(-a\eta k)$.

Oboukov (1949) and Corrsin (1951) argue that the inertial–convective subrange of the scalar-variance spectrum ($1/L < k < k_{oc}$) should be scaled by the scalar dissipation χ, the kinetic-energy dissipation ϵ and the viscosity ν in a manner analogous to Kolmogorov scaling:

$$E_\theta(k) = \alpha_\theta \chi \epsilon^{-\frac{1}{3}} k^{-\frac{5}{3}}. \tag{6}$$

Kolmogorov scaling is obeyed if the Oboukov–Corrsin constant α_θ is universal and independent of Prandtl number when the high Reynolds number scalar-variance spectra are normalized by

$$\frac{\chi}{\epsilon}(\epsilon\nu^5)^{\frac{1}{4}}. \tag{7}$$

The spectrum between the inertial–convective subrange and the scalar-dissipation regime is determined by the Prandtl number and the ordering of the wavenumber cutoffs.

For high Prandtl number (low diffusivity), the wavenumber cutoffs are ordered as

$$k_k < k_B < k_{oc}$$

and Batchelor (1959) predicts that the viscous–convective spectrum, which is between the Kolmogorov wavenumber and the Batchelor wavenumber, obeys

$$E_\theta(k) = \frac{\chi}{|\gamma_3| k} \exp\left[\frac{-k^2\kappa}{|\gamma_3|}\right], \tag{8}$$

where $|\gamma_3|$ is the average value of the least principle rate of strain. The dissipation regime for all Prandtl numbers, like the dissipation regime of the kinetic-energy spectrum, is now believed to be an exponential like $\exp(-k)$, but Kraichnan (1969) suggests that the k^{-1} power law in (8) is rigorous.

For low Prandtl numbers (high diffusivity) the wavenumber cutoffs are ordered as

$$k_{oc} < k_B < k_k.$$

Between k_{oc} and k_k, Batchelor, Howells & Townsend (1959) suggested that the inertial–diffusive spectrum would have the form

$$E_\theta(k) = \tfrac{1}{3}\alpha\chi\kappa^{-3}\epsilon^{\frac{2}{3}}k^{-\frac{17}{3}} \tag{9a}$$

for an ideal $-\frac{5}{3}$ energy spectrum. For an arbitrary energy spectrum the prediction is

$$E_\theta(k) = \tfrac{1}{3}E(k)\,\chi\kappa^{-3}k^{-4}. \tag{9b}$$

However, Gibson (1968*b*) predicts that at intermediate wavenumbers, between k_{oc} and k_B, the spectrum will follow

$$E_\theta(k) = \alpha_G \frac{\chi}{\kappa} k^{-3} \tag{10}$$

and that the $k^{-\frac{17}{3}}$ regime will be valid only between k_B and k_k. The spectral regime between k_{oc} and k_B is labelled the strain-rate-diffusive regime and when normalized by (7) the spectral constant for (10) is $\alpha_G\,\sigma$. Both theories agree that there should be a $-\frac{5}{3}$ inertial–convective regime for wavenumbers below the Oboukov–Corrsin cutoff k_{oc}.

Two secondary predictions based on the theory of Gibson (1968*a*, *b*) are that the mixed-derivative skewness (22) is independent of Prandtl number (Clay 1973) and that in the dissipation regime, scalar spectra will depend only upon the scalar

dissipation χ, the rate of strain $(\epsilon/\nu)^{\frac{1}{2}}$, and the Batchelor scale η_B. With this scaling, scalar dissipation spectra scaled by

$$\chi\left(\frac{\nu}{\epsilon}\right)^{\frac{1}{2}}\eta_B \tag{11}$$

will be independent of the Prandtl number. This is called Batchelor scaling because it was first proposed for large Prandtl numbers by Batchelor (1959).

Theories are usually formulated for three-dimensional spectra, but experimentalists usually present one-dimensional spectra because single hot-wire anemometers measure only the longitudinal one-dimensional kinetic-energy spectrum

$$\phi_1(k_1) = (u_1^2(|k_1|) + u_1^2(-|k_1|)), \tag{12}$$

although with crossed-wire probes the full one-dimensional kinetic-energy spectrum

$$E_1(k_1) = \tfrac{1}{2}(u^2(|k_1|) + u^2(-|k_1|)) \tag{13}$$

can also be measured. In isotropic turbulence these spectra are related to the three-dimensional, kinetic-energy spectrum by

$$\phi_1(k_1) = \int_{k_1}^{\infty}\left(1-\frac{k_1^2}{k^2}\right)\frac{E(k)}{k}\,\mathrm{d}k, \quad E(k) = \frac{k^3}{2}\frac{\mathrm{d}}{\mathrm{d}k}\left(\frac{1}{k}\frac{\mathrm{d}\phi_1}{\mathrm{d}k}\right) \tag{14a, b}$$

and

$$E_1(k_1) = \int_{k_1}^{\infty}\frac{E(k)}{k}\,\mathrm{d}k, \quad E(k) = k\frac{\mathrm{d}E_1(k)}{\mathrm{d}k}. \tag{15a, b}$$

In the inertial subrange $\phi_1(k_1) = \alpha_1\epsilon^{\frac{2}{3}}k_1^{-\frac{5}{3}}$ and $E_1(k_1) = \alpha_1'\epsilon^{\frac{2}{3}}k_1^{-\frac{5}{3}}$, where the one-dimensional Kolmogorov constants are

$$\alpha_1' = \tfrac{3}{5}\alpha, \quad \alpha_1 = \tfrac{18}{55}\alpha. \tag{16a, b}$$

In Kerr (1985*b*) some full one-dimensional kinetic-energy spectra (13) for these simulations are plotted along with one experimental curve, but here only the longitudinal spectra (12) are discussed because more experiments are available for comparisons over a wider range of Reynolds numbers.

The one-dimensional scalar-variance spectrum, which can be measured with a single temperature probe, is related by isotropy to the three-dimensional spectrum by

$$\Gamma(k_1) = \int_{k_1}^{\infty}\frac{E_\theta(k)}{k}\,\mathrm{d}k, \quad E_\theta(k) = k\frac{\mathrm{d}\Gamma(k)}{\mathrm{d}k}. \tag{17a, b}$$

In the inertial subrange $\Gamma(k_1) = \alpha_{\theta 1}\chi\epsilon^{-\frac{1}{3}}k_1^{-\frac{5}{3}}$, where the one-dimensional Oboukov–Corrsin constant is

$$\alpha_{\theta 1} = 0.6\alpha_\theta. \tag{18}$$

A major aim of turbulence theory is to successfully predict the constants for these spectral subranges, while an objective of the experimentalists is to provide the theorists with reliable values for the constants. One approach to making theoretical predictions is to use a spectral closure. For example, Herring & Kraichnan (1979) use a variant of the direct-interaction approximation (DIA, Kraichnan 1959) and calculate the three-dimensional Kolmogorov constant to be 1.72. Some comparisons between these simulations and eddy-damped quasi-normal Markovian model predictions (EDQNM, Orszag 1970) from Herring *et al.* (1982) are discussed here to show where differences between these results and high Reynolds number turbulence are expected.

Another theoretical approach is to make assumptions about the cascade of energy to high wavenumbers. If the cascade is space-filling one expects a $k^{-\frac{5}{3}}$ inertial subrange. But it is well known that the dissipation is intermittent and by making assumptions about spatial intermittency Kolmogorov (1962) and Frisch, Sulem & Nelkin (1978) predict small corrections to the $-\frac{5}{3}$ law. Siggia (1978) and Kerr & Siggia (1978) discuss temporal intermittency, but make no spectral predictions. It will be shown that temporal intermittency qualitatively similar to that observed by Kerr & Siggia (1978) is an important aspect of the simulated spectra.

One topic that is not discussed here is the helicity $H = \boldsymbol{u}\cdot\boldsymbol{\omega}$. Kerr (1987) shows that the velocity forcing used for these simulations is strongly helical, but that helicity does not play a strong role in the energy cascade. Whether this has a strong effect on the spectra to be discussed can only be determined by doing calculations where the forcing has zero helicity. To determine whether the helicity provides any constraint upon the energy cascade and to determine the direction of the helicity cascade, helicity transfer spectra would need to be calculated.

2. Numerical method

The governing equations of the simulation are the incompressible Navier–Stokes equation for the velocity and the transport equation for a passive scalar. The Navier–Stokes equation is

$$\frac{\partial \boldsymbol{u}}{\partial t} + \boldsymbol{u}\cdot\boldsymbol{\nabla}\boldsymbol{u} = -\frac{\boldsymbol{\nabla} p}{\rho} + \nu\nabla^2\boldsymbol{u}, \tag{19}$$

$$\boldsymbol{\nabla}\cdot\boldsymbol{u} = (0 \quad \text{incompressibility}),$$

and the convective form of the scalar equation is

$$\frac{\partial \vartheta}{\partial t} + \boldsymbol{u}\cdot\boldsymbol{\nabla}\vartheta = \kappa\nabla^2\vartheta. \tag{20}$$

In the absence of viscosity ν and diffusivity κ the equations conserve two positive-definite quadratic invariants: the kinetic energy of turbulent fluctuations $E = \frac{1}{2}\langle u_i u_i\rangle$; and the scalar variance $E_\theta = \langle\theta^2\rangle$. The fundamental dimensionless parameters that determine our spectra are the Taylor-microscale Reynolds number, $R_\lambda = U\lambda/\nu$, and the Prandtl number $\sigma = \nu/\kappa$, where U is the characteristic velocity of the turbulence, $\frac{3}{2}U^2 = E$ and $\lambda = \langle u_1^2\rangle^{\frac{1}{2}}/\langle(\partial u_1/\partial x_1)^2\rangle^{\frac{1}{2}}$ is the Taylor microscale. The time span of the statistical samples to be discussed should be compared with the eddy-turnover time

$$t_e = \frac{L}{U}, \quad \text{where} \quad L = \frac{3\pi}{4E}\int k^{-1}E(k)\,\mathrm{d}k \tag{21a, b}$$

is the integral lengthscale of the flow (Batchelor 1971).

The numerical code used is a three-dimensional pseudospectral code with periodic boundary conditions, 128^3 mesh points, and no subgrid modelling of the small scales. With a large-scale forcing, Taylor-microscale Reynolds numbers as high as 83 can be simulated with full resolution of the smallest scales. Prandtl numbers are restricted in our simulations to less than 1.0 in order to maintain good resolution of the small scales and to greater than 0.1 in order to allow a wide enough range of scales to identify spectral regimes. Details of the simulations are given in the table 1, with the case numbers corresponding to those in Kerr (1985*a*). Additional details about the algorithms, computed usage, aliasing control, and forcing may be found in Kerr (1985*a*).

Run	Mesh	R_λ	σ	k_κ	k_B	k_{oc}	t_e
F22	64^3	55.9	1.0	27.2	27.2	27.2	1.05
F23	64^3	55.9	0.5	27.2	19.2	16.2	1.05
F24	64^3	55.9	0.1	27.2	8.6	4.8	1.05
F25	128^3	82.9	1.0	45.7	45.7	45.7	0.85
F26	128^3	82.9	0.5	45.7	32.3	27.2	0.85
F27	128^3	82.9	0.1	45.7	14.5	8.1	0.85

TABLE 1. Characteristics of the simulations

Because the equations are forced, a statistically steady state can be maintained and time averages of the spectra obtained. Figures 1–8 represent averages over at least two eddy-turnover times for each Reynolds number. To show Kolmogorov scaling figures 1–7 have been normalized by the Kolmogorov microscales and scalar dissipation (5), (7) and have been multiplied by $k^{\frac{5}{3}}$ so that the inertial subrange would appear as a line with zero slope in these figures. Figure 8 uses Batchelor scaling (11).

The wavenumbers included in a three-dimensional wavenumber shell k_0 are all $\boldsymbol{k}$ such that $k_0 \leqslant |\boldsymbol{k}| < k_0 + 1$. One problem with the calculation of the three-dimensional spectrum is that the number of modes in each shell is not a smooth function of wavenumber. To produce a smoother curve, the energy in each shell of the three-dimensional spectra to be discussed has been divided by the number of modes in the shell and multiplied by the volume of the shell, $\frac{4}{3}\pi((k_0+1)^3 - k_0^3)$. The wavenumber plotted has been weighted by an estimate of the energy within each shell. For the first, forced shell, the plotted wavenumber is $\frac{3}{2}$. For the higher shells the weight uses the root-mean-square of a $k^{-\frac{5}{3}}$ spectrum summed over the modes within a shell. These weightings have been applied to figures 1, 2, 4, 6, 7 and 8.

3. Velocity spectra

Figure 1 replots figure 2 of Kerr (1985*a*) using the weighting just described and a log–log scale to compare the calculated, three-dimensional, kinetic-energy spectra and scalar-variance spectra for several Prandtl numbers. In this figure the highest Reynolds number kinetic-energy spectrum appears to have one decade of a Kolmogorov inertial subrange with a Kolmogorov constant of about 2. While this is encouraging, to prove consistency with the Kolmogorov hypothesis, simulated spectra for several Reynolds numbers should collapse to a single curve. To show the trends in this direction figure 2 uses a linear-logarithmic scale to plot kinetic-energy spectra for all four simulated Reynolds numbers. Except for the lowest Reynolds number, all of the spectra in figure 2 collapse to a single form in the dissipation regime that agrees with the EDQNM calculation of Herring *et al.* (1982). Below the dissipation regime ($\eta k < 0.4$), the spectra seem to be approaching a limit as the Reynolds number increases, but figure 2 does show that the inertial subrange plotted in figure 1 is partially an illusion due to the plotting technique. Although figure 2 does not show a well-defined inertial subrange, the short inertial range that is seen suggests that there is a realistic turbulence cascade feeding the dissipation regime.

To get better comparisons with experiment, one-dimensional spectra must be plotted. Figure 3 presents the calculated, longitudinal, one-dimensional, kinetic-energy spectrum (12) for our two highest Reynolds numbers and comparisons with several experiments. In the dissipation range the computed and low Reynolds

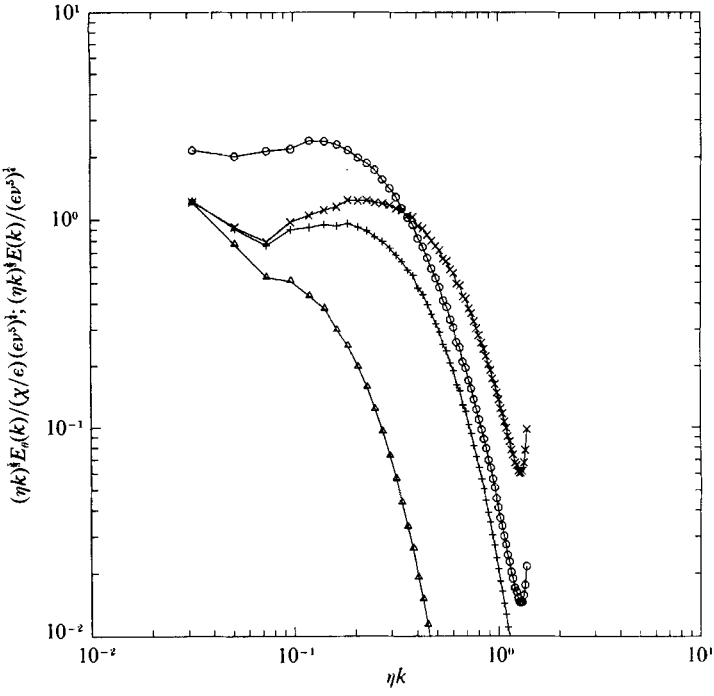

FIGURE 1. Three-dimensional kinetic-energy and passive-scalar spectra for $R_\lambda = 82.9$ normalized by the Kolmogorov microscales and the scalar-variance dissipation, χ, (5), (7) and multiplied by $k^{\frac{5}{3}}$. ○, kinetic energy; ×, $\sigma = 1.0$; +, $\sigma = 0.5$; △, $\sigma = 0.1$.

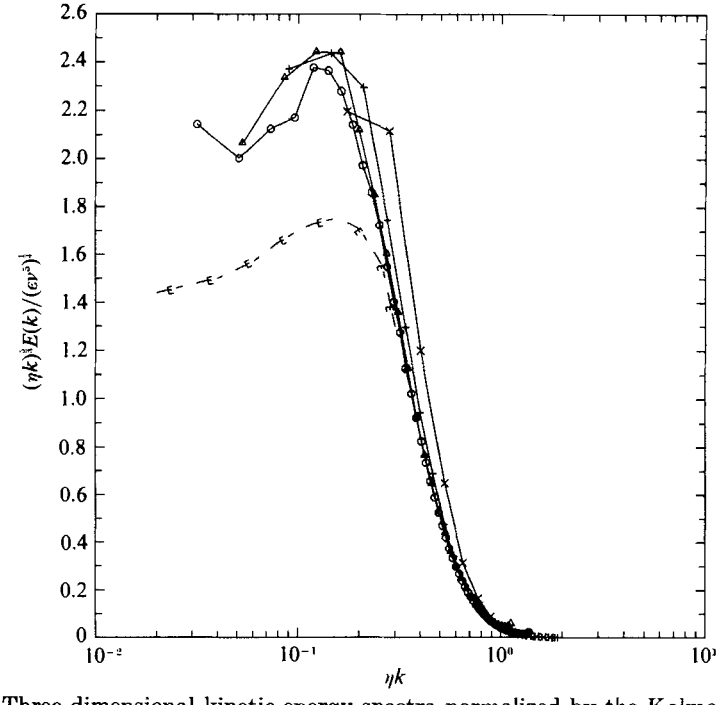

FIGURE 2. Three-dimensional kinetic-energy spectra normalized by the Kolmogorov microscales and (5) and multiplied by $k^{\frac{5}{3}}$. ○, $R_\lambda = 82.9$; △, $R_\lambda = 55.9$; +, $R_\lambda = 37.2$; ×, $R_\lambda = 18.4$; E, EDQNM calculation by Herring *et al.* (1982). The logarithmic-linear scale is used to show the convergence properties.

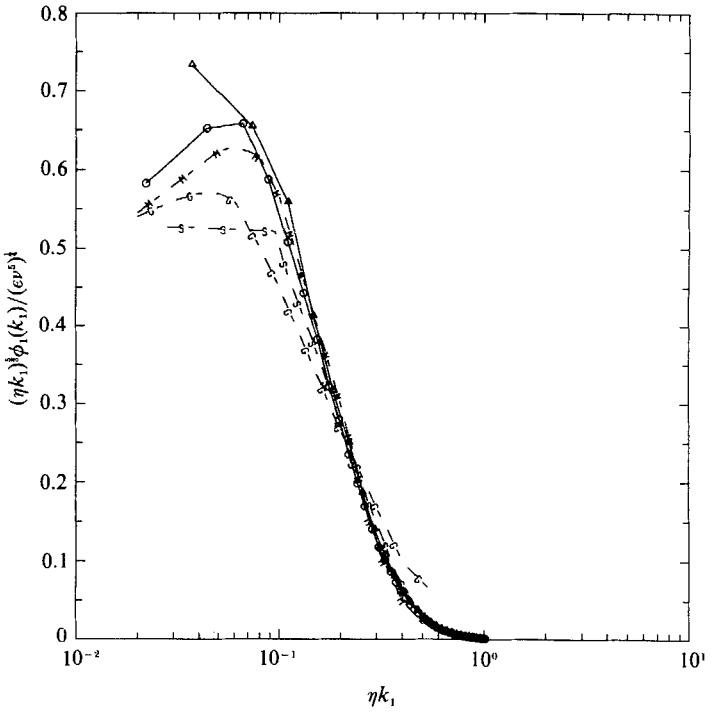

FIGURE 3. Longitudinal one-dimensional kinetic-energy spectra normalized by the Kolmogorov microscales and (5) and multiplied by $k^{\frac{5}{3}}$. ○, $R_\lambda = 82.9$; △, $R_\lambda = 55.9$. Experimental spectra are M, Mestayer *et al.* (1983) at $R_\lambda = 561$; S, Champagne (1978), $R_\lambda = 130$; and G, Champagne *et al.* (1977) $R_\lambda = 13000$.

number experimental spectra agree closely, supporting the claim of Kerr (1985*a*) that this simulation reproduces the statistics of the dissipation regime. In the inertial subrange the computations and experiments do not agree, although both the computations and two low Reynolds number experiments by Mestayer, Chollet & Lesieur (1983) and Champagne (1978) have Kolmogorov constants that are higher than the generally accepted value of about $\alpha = 1.5$ or $\alpha_1 = 0.49$ (Champagne 1978). The data from Mestayer *et al.* (1983), labelled there as ME.MO.MI.IV2, are at $R_\lambda = 561$ and agree particularly well with the simulations. The data from Champagne (1978) are for a homogeneous shear at $R_\lambda = 130$. In Kerr (1985*a*, *b*) this anomalously large Kolmogorov constant was attributed to a bump that has been seen in some high Reynolds number experiments of Champagne (1978) and theoretical predictions such as EDQNM calculations discussed in Mestayer *et al.* (1983). But the comparisons with low Reynolds number experiments now suggest that most of the anomalously large Kolmogorov constant in these computations is due to the low Reynolds number effect discussed above.

Although only low Reynolds number experimental spectra can properly be compared with the numerical results, because theory and closures suggest that dissipation spectra should be universal, figure 3 includes one high Reynolds number experimental curve from Champagne *et al.* (1977) at $R_\lambda = 13000$. The anomalously high Kolmogorov constant is the bump discussed by Kerr (1985*a*, *b*). At wavenumbers below those plotted the Kolmogorov constant α_1 is closer to the accepted value of about 0.5 and the difference in the far dissipation regime between

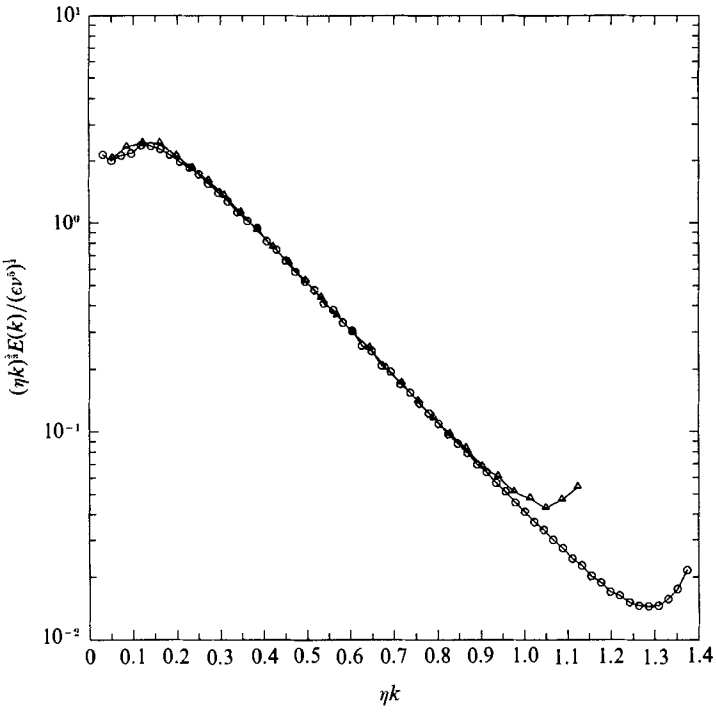

FIGURE 4. Three-dimensional kinetic-energy spectra normalized by the Kolmogorov microscales and (5) and multiplied by $k^{\frac{5}{3}}$. ○, $R_\lambda = 82.9$; △, $R_\lambda = 55.9$; +, $R_\lambda = 37.2$; ×, $R_\lambda = 18.4$. E is an EDQNM calculation by Herring *et al.* (1982). The linear-logarithmic scale is used to show the exponential dissipation tail.

this spectra and the low Reynolds number experimental and simulated spectra is consistent with a set of older data compiled by Chapman (1979) that was used for comparison by Kerr (1985*b*). If a correction to the Taylor frozen-turbulence assumption suggested by Lumley (1965), and implemented by Champagne (1978), were shown, the difference in the dissipation regime would be less, but still significant.† From comparisons of figures 2 and 3 it can be seen that there is also a difference in the dissipation regime between Champagne *et al.* (1977) and the predictions of EDQNM, both of which are supposed to be high Reynolds number results. These differences suggest that either some aspect of measuring high Reynolds number spectra is not understood or that the universality of Kolmogorov scaling for dissipation spectra is limited.

Figure 4 uses a logarithmic-linear scale to plot the three-dimensional kinetic-energy spectra for $R_\lambda = 56$ and 83 because on the basis of analyticity arguments referenced it is believed that the far dissipation regime should be a simple exponential. Our data support that conclusion with $B = 6.5 \pm 0.1$ and $a = 5.1 \pm 0.1$ when $B\exp(-a\eta k)$ is fitted to $(\eta k)^{\frac{5}{3}}E(k)/(\epsilon\nu^5)^{\frac{1}{4}}$. This is consistent with values of $B = 8.4 \pm 0.6$ and $a = 4.9 \pm 0.1$ found by Kida & Murakami (1987) for a symmetrized decaying calculation. They also make comparisons with experimental data by Sreenivasan (1985).

† Mestayer *et al.* (1983) contends that this correction should not be used.

4. Passive-scalar variance spectra

In the previous section it was shown that the dissipation regime of the kinetic-energy spectrum converges and agrees with experiments. This suggests that this simulation can be reliably used to study scalar-dissipation spectra, even though supporting experimental evidence for scalars is poor and cannot be used to verify the simulation. Because there is evidence for an inertial subrange in the velocity spectrum, qualified comparisons in figure 1 between scalar regimes for three Prandtl numbers, $\sigma = 0.1$, 0.5, and 1.0, that overlap the inertial subrange can also be justified. To present different aspects of the scalar-variance spectra for the three Prandtl numbers in more detail figures 5–7 plot spectra for several Reynolds numbers. Kolmogorov scaling (7) is used for all the scalar-variance spectra in figures 1, 5–7.

Figure 5 shows the one-dimensional spectra for the two largest Reynolds numbers for $\sigma = 0.1$ along with two theoretical predictions. The curve labelled B uses the full one-dimensional kinetic-energy spectrum (13) for $R_\lambda = 83$ in the second form of the $k^{-\frac{17}{3}}$ prediction (9*b*). The curve labelled *G* uses the k^{-3} prediction of (10) with a one-dimensional constant of 0.07, or $\alpha_G = 2.1$. For $\sigma = 0.02$ (liquid mercury), Clay (1973) finds some evidence for a $-\frac{17}{3}$ regime and an intermediate regime that would be consistent with the k^{-3} regime predicted by Gibson (1968*b*). Neither of these regimes appears distinctly in figure 5, which is not surprising because the three spectral cutoffs (3*a–c*) should be widely spaced in order to observe the predicted low Prandtl number regimes, and this would require high Reynolds numbers and low Prandtl numbers. For the $R_\lambda = 83$ calculation the k_{oc}, k_B and k_k wavenumber cutoffs are at $\eta k = 0.18$, 0.32 and 1.0 respectively in figure 5. In addition all of these regimes overlap the poorly defined inertial subrange and are probably strongly influenced by the problems with the scalar forcing to be discussed next. Nevertheless, because it is difficult to make these measurements experimentally and because secondary predictions of the theory of Gibson are supported by this simulation and experiments, some comment is valid. One-dimensional spectra are plotted in figure 5 in order to allow easier comparisons with future experiments and to minimize the difficulties with normalizing three-dimensional spectra and the errors introduced by the forcing.

The first point is that an inertial–convective subrange (6) for wavenumbers below the Oboukov–Corrsin cutoff k_{oc} is not found in figure 5, even though k_{oc} is within the simulation. This is expected because the dissipation peak of the velocity spectrum typically occurs closer to $0.2k_k$ than the order of magnitude estimate k_k and all spectral regimes might be expected to be found at lower wavenumbers than their order of magnitude estimates would predict. The second point is that while the $-\frac{17}{3}$ prediction does match the simulations at very large wavenumbers and is consistent with Chasnov, Canuto & Rogallo (1988), there is a long transition from this regime to the lowest wavenumber of the calculation that would be consistent with the strain-rate-diffusive prediction of Gibson (1968*b*). The transition wavenumber where the prediction of (9*b*) begins to depart from the simulated spectra is very close to the Batchelor cutoff (3*b*) of $\sigma^{\frac{1}{2}}\eta$, or 0.32η for $\sigma = 0.1$, as predicted by Clay (1973). While this alone is not sufficiently strong evidence to favour the -3 prediction of Gibson (1968*b*), figure 8 will present evidence for one of the secondary predictions of that theory. In addition, Kerr (1985*a*) finds that the mixed-derivative skewness

$$S_{u\theta} = \left\langle \frac{\partial u_l}{\partial x_1}\left(\frac{\partial \theta}{\partial x_1}\right)^2 \right\rangle \Big/ \left[\left\langle \left(\frac{\partial u_1}{\partial x_1}\right)^2 \right\rangle^{\frac{1}{2}} \left\langle \left(\frac{\partial \theta}{\partial x_1}\right)^2 \right\rangle \right] \tag{22}$$

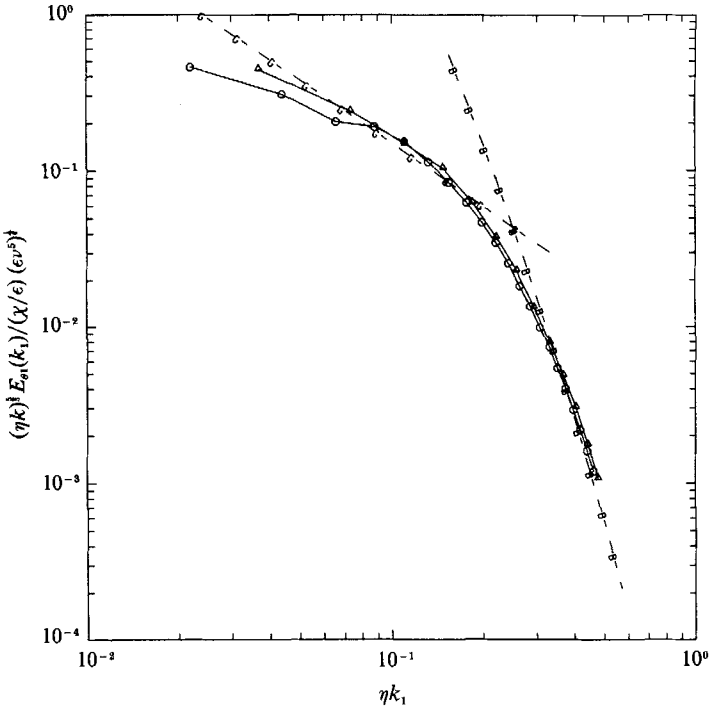

FIGURE 5. One-dimensional passive scalar spectra for $\sigma = 0.1$ normalized by the Kolmogorov microscales and the scalar-variance dissipation χ with (7), and multiplied by $k^{\frac{5}{3}}$. ○, $R_\lambda = 82.9$; ×, $R_\lambda = 55.9$. First mode is not plotted for each R_λ. B, $-\frac{17}{3}$ prediction (9*b*); G, -3 prediction (10) with $\alpha_G = 2.1$.

is independent of both the Reynolds number and Prandtl number and equal to -0.5 in these simulations, which is consistent with a prediction of Clay (1973) that is based on the theory of Gibson (1968*a*, *b*). Gibson & Kerr (1987) discusses this and additional computational and experimental evidence that supports that theory.

To get better comparisons with the low Prandtl number theories a wider range of scales needs to be simulated. This requires larger Reynolds numbers, since simply lowering the Prandtl number on a 128^3 mesh with a low wavenumber forcing would put the Oboukov–Corrsin wavenumber k_{oc} in the regime where the forcing dominates. Increasing the Reynolds number on a 128^3 mesh would imply sacrificing some small-scale resolution, but this should not affect the behaviour at the Oboukov–Corrsin scale η_{oc} and Batchelor scale η_B when the Prandtl number is small.

In figure 6 three-dimensional scalar-variance spectra are plotted for $\sigma = 0.5$ for the same four calculations and Reynolds numbers used in figure 2. A linear scale is used for the scalar variance to show how well scalar-variance spectra converge for different Reynolds numbers and determine whether a $-\frac{5}{3}$ inertial–convective subrange has been calculated. It is important to use a linear scale for at least one Prandtl number, just as it was important for the velocity in figure 2, and $\sigma = 0.5$ is used for this demonstration because no subranges in the scalar-variance spectrum are expected besides the dissipative range and the $-\frac{5}{3}$ inertial-convective subrange (6), for which there is some evidence in figure 1. Figures 4 and 6 in Kerr (1985*b*) show similar scaling properties for $\sigma = 0.1$ and 1.0 at all the simulated Reynolds numbers. As was true for the velocity, in the dissipation regime the higher Reynolds number

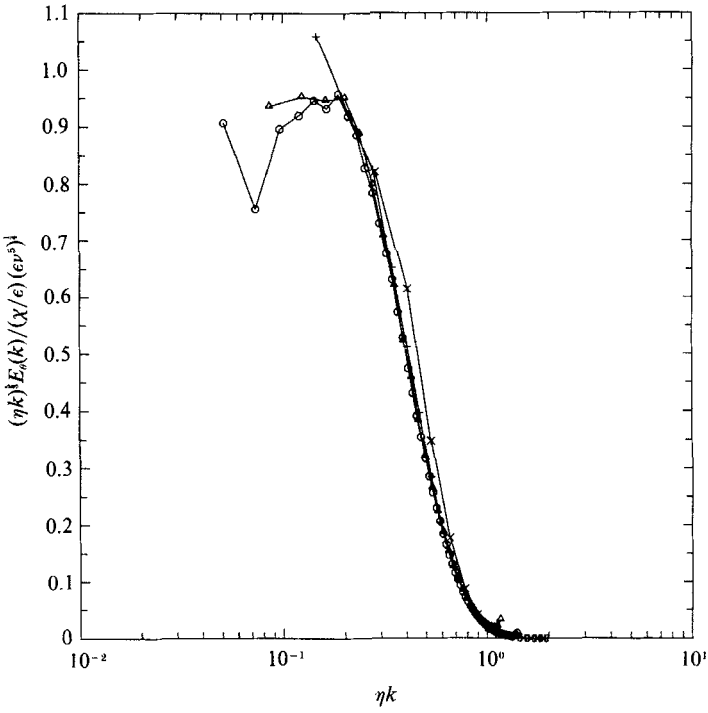

FIGURE 6. Three-dimensional passive-scalar spectra for $\sigma = 0.5$ normalized by the Kolmogorov microscales and the scalar-variance dissipation χ with (7) and multiplied by $k^{\frac{5}{3}}$. First mode is not plotted for each R_λ. ○, $R_\lambda = 82.9$; △, $R_\lambda = 55.9$; +, $R_\lambda = 37.2$; ×, $R_\lambda = 18.4$. The logarithmic-linear scale is used to show the convergence properties.

spectra converge to a form that is independent of Reynolds number. But in the inertial–convective subrange the convergence is poorer for the scalar than it was for the velocity in the inertial subrange. Part of this might be related to the forcing since at the third wavenumber shell there is a sharp break for each Reynolds number in figure 6 and for the other Prandtl numbers in figure 1. The best value for the $-\frac{5}{3}$ Oboukouv–Corrsin constant from figure 6 would be $\alpha_\theta = 1.0$, or about half the Kolmogorov constant. The one-dimensional constant, $\alpha_{\theta_1} \approx 0.6$, (18), is consistent with a wide range of experimental values (Champagne *et al.* 1977; references in Pao 1965; Clay 1973 and Monin & Yaglom 1975, p. 511). Figure 1 shows that at low wavenumbers, spectra for $\sigma = 0.1$ and 1.0 might be converging to a similar value for α_θ. This is expected if the value of the scalar diffusivity κ does not have a significant effect on the inertial–convective subrange.

For high Prandtl numbers (low scalar diffusivity) there is strong experimental support for a k^{-1} subrange (8) (see Monin & Yaglom 1975, p. 513). $\sigma = 1.0$ (figure 7) is too low for this subrange, shown by the curve labelled B, to be observed fully, but scalar experiments for $\sigma = 0.7$ (air) show a 'bump' that looks like a short k^{-1} (Hill 1978). Therefore, it is not surprising that a significant bump is observed in our calculated spectra for $\sigma = 1.0$. An EDQNM theoretical prediction is shown for comparison.

While Kolmogorov scaling might be independent of Prandtl number in the inertial–convective subrange, figure 1 shows that it does not apply to the dissipation regime, which is where the effect of Prandtl number is largest. Gibson (1968*b*)

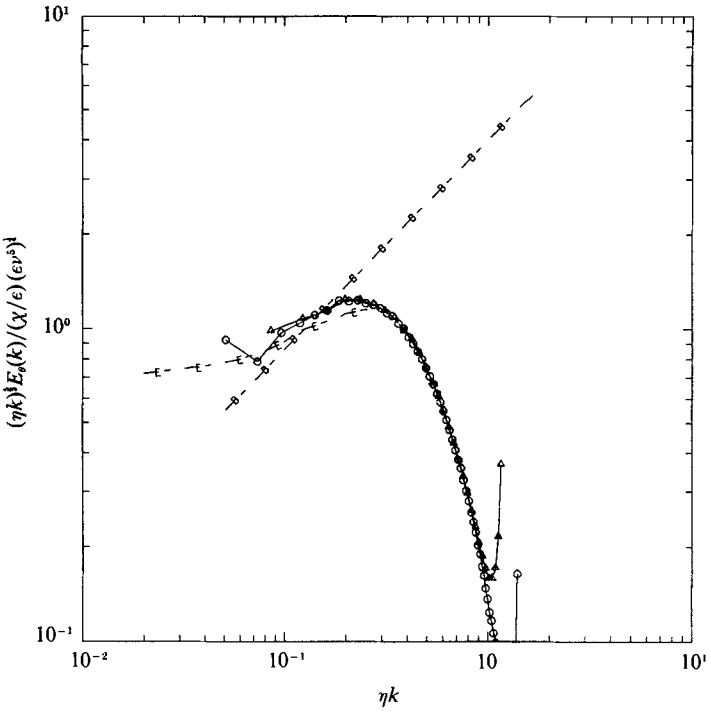

FIGURE 7. Three-dimensional passive-scalar spectra for $\sigma = 1.0$ normalized by the Kolmogorov microscales and the scalar-variance dissipation χ with (7) and multiplied by $k^{\frac{5}{3}}$. First mode is not plotted for each R_λ. ○, $R_\lambda = 82.9$; △, $R_\lambda = 55.9$; B, -1 prediction (8) with arbitrary coefficient; E, EDQNM calculation by Herring *et al.* (1982).

predicts instead that in the dissipation regime, Batchelor scaling (11), which is independent of Prandtl number, is obeyed, a prediction that is supported by the experiments of Clay (1973) for Prandtl numbers from 0.02 (liquid mercury) to 7.0 (water). Figure 8 replots the scalar spectra in figure 1 to show that this scaling also applies to the computational spectra for $\sigma = 0.1$ to 1.0 and Gibson & Kerr (1987) show that the experimental spectra of Clay (1973) and the computational spectra agree in the dissipation regime. Figure 8 is plotted on a logarithmic-linear scale to emphasize the exponential tail of the scalar spectra in the dissipation regime. Close comparison of figure 4 for the velocity and figure 8 suggests that, if an exponential tail has any validity for the scalars, substantial corrections are necessary. The best fit to $\exp(-a\eta_B k)$ has $a = 3.3 \pm 0.2$. Recall that (8) predicts k^2 in the exponential.

The theory that predicts Batchelor scaling is fundamentally based upon the assumption that at high wavenumbers the large-scale strain acting on relatively long timescales can dominate the scalar dissipation even though inertial range arguments such as Batchelor *et al.* (1959) suggest that a local, small-scale timescale should be used. Mechanistic models such as hot-spot pinching that incorporate this assumption are probably not an essential part of the original theory of Gibson (1968*b*). In fact Gibson, Ashurst & Kerstein (1988) finds that most of the mixed-derivative skewness in a two-dimensional simulation can be directly attributed to another mechanism which they label large-gradient-pinching. At low Prandtl numbers the assumption of Batchelor scaling can be valid only if the rate of strain is constant over scales large compared with Kolmogorov microscale η. This claim would be consistent with the

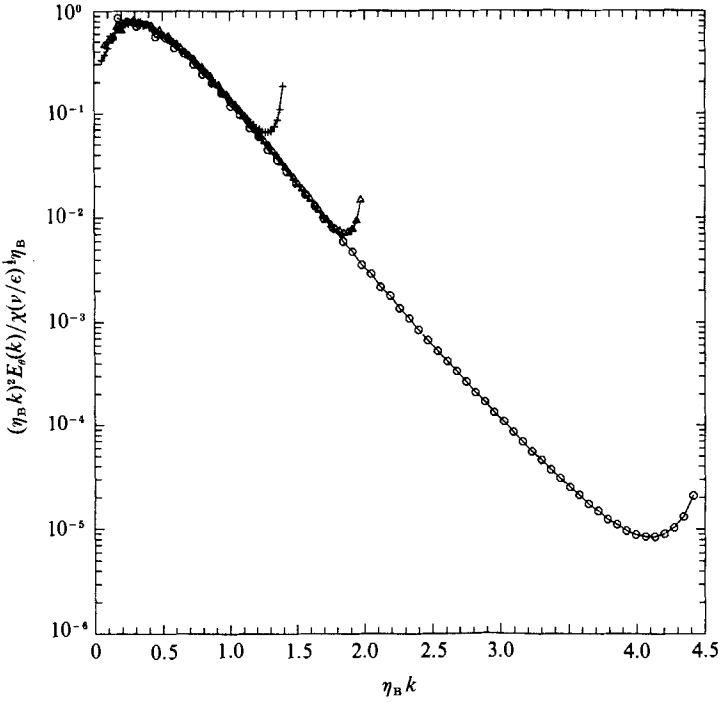

FIGURE 8. Three-dimensional passive-scalar spectra for $R_\lambda = 82.9$ normalized by the Batchelor microscale, the scalar-variance dissipation χ, and strain (11). First mode is not plotted for each σ. ○, $\sigma = 0.1$; △, $\sigma = 0.5$; +, $\sigma = 1.0$. The linear-logarithmic scale is used to show the exponential dissipation tail.

graphics of Kerr (1985*a*) where scalar-gradient structures are aligned with extended vortex structures whose large scale is several times η. Finding that Batchelor scaling is valid for all Prandtl numbers is aesthetically pleasing because only one scaling is required, rather than two as originally suggested by Batchelor (1959) and Batchelor *et al.* (1959).

5. Energy-transfer spectra

Another spectrum that can be investigated only marginally with experiments, but can be determined exactly by simulations (Van Atta 1979), is the transfer spectrum, that is the rate at which energy is transferred, or cascades, into or out of a wavenumber band. The three-dimensional energy-transfer spectrum $T_u(k)$ is defined by the equation for the three-dimensional kinetic-energy spectrum

$$\frac{\mathrm{d}}{\mathrm{d}t}E(k) = T_u(k) - 2\nu k^2 E(k). \tag{23}$$

The integral of the energy-transfer spectrum is zero, $\int T_u(k)\,\mathrm{d}k = 0$ (where the limits of all our integrals are from 0 to ∞), but the integral of the enstrophy-production, or mean-square vorticity-production, spectrum

$$P_\Omega = \int k^2 T_u(k)\,\mathrm{d}k \tag{24}$$

is non-zero and in isotropic turbulence is related to the velocity-derivative skewness

$$S_u = \left\langle \left(\frac{\partial u_i}{\partial x_1}\right)^3 \right\rangle \Big/ \left\langle \left(\frac{\partial u_1}{\partial x_1}\right)^2 \right\rangle^{\frac{3}{2}} \tag{25}$$

by

$$-S_{u(k)} = \frac{2}{35} \frac{P_\Omega}{(\epsilon/15\nu)^{\frac{3}{2}}}. \tag{26}$$

For our forced simulations, an extra source term is added, but it appears at low wavenumbers and has negligible effect on the enstrophy production and velocity-derivative skewness.

In Kerr (1985*a*), the transfer spectra were used with these equations, and similar equations for the scalar variance, to calculate the enstrophy production and scalar-dissipation production, and in turn the velocity-derivative skewness (25) and the mixed-derivative skewness (22). Here the three-dimensional energy-transfer spectrum $T_u(k)$ and the enstrophy-production spectra $k^2 T_u(k)$ are used to highlight temporal fluctuations in the velocity field in wavenumber space. Production spectra are used in some of the figures instead of transfer spectra because the extra k^2 factor emphasizes high wavenumbers more, but the same conclusions apply to the transfer spectra. In this analysis complete energy-transfer spectra for many different times will be given first. Then time correlations of the production spectra between different wavenumbers will be plotted to demonstrate the existence of pulses. Finally, time correlations of the dissipation spectra between different wavenumbers will be plotted to show the relationship of the pulses in the production spectra to correlations in the dissipation spectra.

Figure 9 plots the time evolution of the three-dimensional energy-transfer spectra for our largest Reynolds number simulation (F25) over a period of 1.4 eddy-turnover times t_e (21*a*). Similar behaviour is shown for simulation F22 in Kerr (1985*b*). The time span is given in simulation variables and should be compared with the eddy-turnover times in table 1. The transfer out of the first wavenumber band, which is always negative, has been divided by the magnitude of its time-averaged value so that it will fit in the figure, and the time-averaged energy-transfer spectrum is given at the top. Note the smooth behaviour of the time-averaged spectra as opposed to the bursting behaviour at individual times. The sign of the time-averaged spectrum is consistent with a Kolmogorov cascade. That is, in the lowest wavenumber band, which is the energy source, the spectrum is large and negative and at higher wavenumbers the spectrum is positive and almost constant until the dissipation regime. This is expected because in a statistically steady flow where $(\mathrm{d}/\mathrm{d}t)E(k) = 0$ the time-averaged transfer spectrum will equal the dissipation spectrum and have a profile similar to figure 1. Because the integral of the transfer is zero the negative transfer out of the first, forced shell will equal the sum of the positive transfers into the other shells.

This behaviour, while consistent with the general phenomenology of a turbulent cascade, is not consistent with a steady cascade of energy to high wavenumber. In Kerr (1985*b*) the intermittent behaviour of the time-dependent transfer spectra was ascribed to pulses that propagate to higher wavenumber with time and lines were drawn to show how individual pulses move. Here that is left to the imagination of the reader and a more quantitative method is used to demonstrate the existence of the pulses.

What is wanted is a way to show correlations between different wavenumbers at

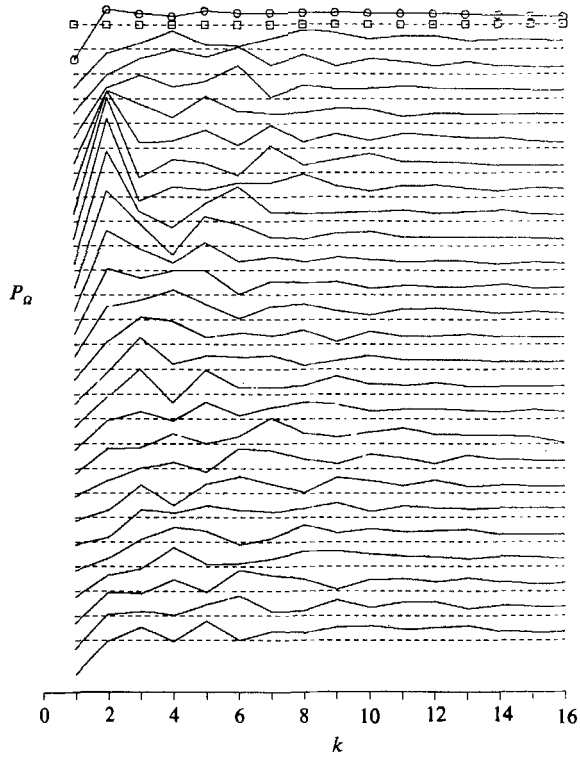

FIGURE 9. Three-dimensional enstrophy-production spectra for discrete times for simulation F25, $R_\lambda = 82.9$. Dashed lines indicate the wavenumber axis for each time. Solid lines indicate the spectra. Squares are the wavenumber axis for the time-averaged transfer spectrum. Circles are the time-averaged spectrum. The lowest mode for each spectrum is normalized by its time-averaged value. The figure spans simulation times from $t = 2.1$ to 3.3, with time increasing from bottom to top. This should be compared to the eddy-turnover time $t_e = 0.85$.

different times that will show any correlations above the generally positive background associated with the time-averaged transfer. To do this

$$\Delta P_\Omega(k_0, t_0) = P_\Omega(k_0, t_0) - \langle P_\Omega(k_0) \rangle, \tag{27}$$

where the brackets indicate an average over time, is compared with $\Delta P_\Omega(k_1, t_1)$ for the 128^3 spectra in figure 10. Because the simulation is analytically steady t_1 can be replaced by $t_0 + \Delta t$, but because it is not known how the correlations scale in wavenumber, k_1 cannot be replaced by $k_0 + \Delta k$ and correlations must be obtained for every wavenumber shell. The correlations are normalized by the variance of the enstrophy production at the two wavenumbers. Contour maps of

$$\frac{\langle \Delta P_\Omega(k_0, t_0)\, \Delta P_\Omega(k_1, t_0 + \Delta t) \rangle}{\langle (\Delta P_\Omega(k_0, t))^2 \rangle^{\frac{1}{2}} \langle (\Delta P_\Omega(k_1, t))^2 \rangle^{\frac{1}{2}}} \tag{28}$$

are shown for wavenumbers $k_0 = 2$–7 with $k_0 = 4$ and 5 demonstrating the appearance of pulses most strongly. Presumably, the pulses are not as strong for low and high k_0 owing to interference with the forcing and dissipation. Figure 10(*c*) shows that within the fluctuations of figure 9 there is a strong correlation which stays as large as 0.5 between different wavenumbers at different times, despite the large statistical sample at moderate wavenumbers ($k \leqslant 10$) in the 128^3 simulation. If

statistics alone governed the size of the pulses, one might expect that their strength would decay as the square root of the sample size. Since the size of each wavenumber shell goes as k^2, this would imply that the pulses should decay as k^{-1}, which, apart from an initial drop from a correlation of 1 at $\Delta k = 0$ and $\Delta t = 0$, is not seen in figure 10(*c*).

Several features of the contour ridges in figure 10 are immediately apparent and require interpretation. These are the positive slope of the ridges, the narrowness of the ridges, where the ridges disappear at large wavenumbers, and their periodicity. The positive slope indicates that there is a forward cascade, but there is an insufficient range of wavenumbers to determine whether the slope would remain constant or change with increasing wavenumber in a higher Reynolds number calculation. A secondary characteristic that follows from a forward cascade is that there is a strong negative ridge at lower wavenumbers, which is equivalent to a later time or positive Δt at the same wavenumber. This represents an energy drain that feeds the strong positive ridge. The narrow width of the peaks is consistent with studies of wavenumber triads (Kraichnan 1976) that have been used to support assumptions of locality. But because these studies of triads effectively consider only $\Delta t = 0$ in figure 10, they are not inconsistent with non-local correlations between large Δt and Δk. Non-locality has been considered in two recent spectral models. Yakhot & Orszag (1986) have used non-locality in their spectral model to support renormalization arguments and Kriachhan (1987) shows how non-locality can enhance the energy cascade in spectral closures and states that, if this property extends to the true Navier–Stokes dynamics, it might be related to flow structures that have strong correlations over several octaves in scale size. This suggests that, rather than continue the analysis of isotropic simulations such as this, a more fruitful approach is to investigate simple models for vortex interaction that have demonstrated non-local transfer and compare them with these results. This is discussed below.

The effect of dissipation is evident in figure 10(*b–f*) as the strong central peak disappears at $k_1 = 10$ or $\eta k_1 = 0.22$. The strong fluctuations in figure 9 also disappear at $k = 10$. If one imagines multiplying the kinetic-energy spectrum in figure 1 by an extra factor of $k^{\frac{1}{3}}$ it can be seen that this is also where the peak of the dissipation spectrum is. The periodic behaviour of the correlation in time for $k_0 = 4$ and 5 occurs on half an eddy-turnover time, which would be consistent with pulses forming from the low-wavenumber forcing on a convective timescale. The periodicity in wavenumber would then be determined by this periodicity and the rate the pulses move to high wavenumber, which is determined by the slopes of the ridges. Another possible explanation is that the periodicity is due to a periodic forcing, but Kerr (1985*a*) looked for periodicity in the forcing and while the samples were short, it was concluded that the forcing acted chaotically.

Figure 11 uses the same correlation technique to compare the energy-dissipation spectrum at different times and wavenumbers for $k_0 = 4$. Dissipation spectra at different times are not plotted in the manner of figure 9 because the fluctuations about the time-averaged spectra are so small, as shown by the lack of strong ridges in figure 11. But though sharp pulses in the disspation do not appear, by overlaying figures 10(*c*) and 11 the reader can see that the peak of 0.360 in figure 11 is associated with the strong central ridge in figure 10(*c*).

Similar pulses have been observed before for time-dependent spectra *in simple* spectral models. Kerr & Siggia (1978) present a cascade model of turbulence where each band of wavenumbers with $2^{l-1} < |k| \leqslant 2^l$ is modelled by a single complex

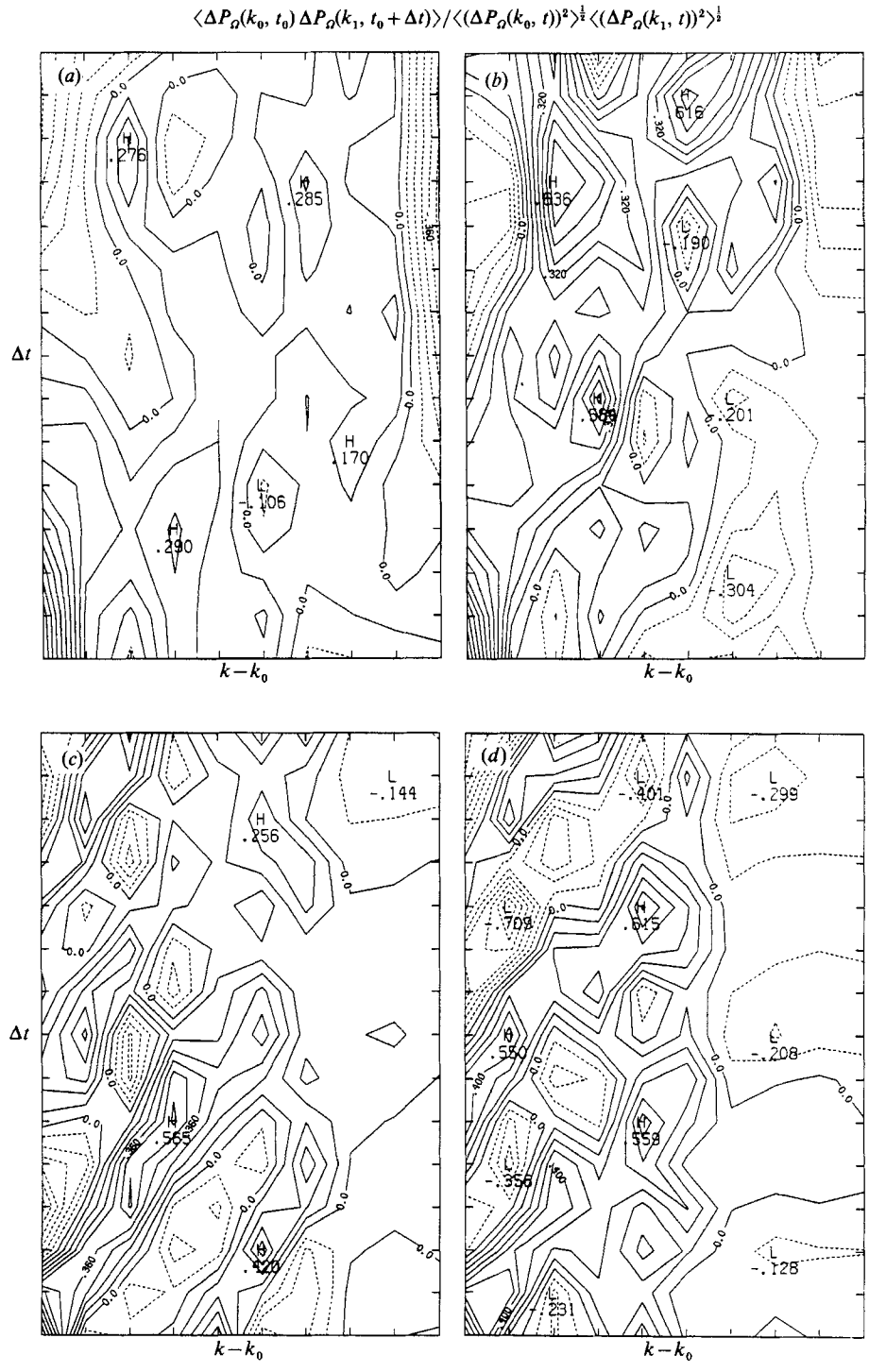

FIGURE 10. Contour plots of time-averaged correlations (28) between three-dimensional enstrophy-production spectra for $k_0 = 2$ to 7 (a to f) respectively, and k_1 for time separations Δt from simulation F25. The sample is from $t = 1.15$ to 3.2 and Δt is from 0 to 0.7. Times should be compared to the eddy-turnover time $t_e = 0.85$. Solid lines are positive contours and dashed lines are negative contours.

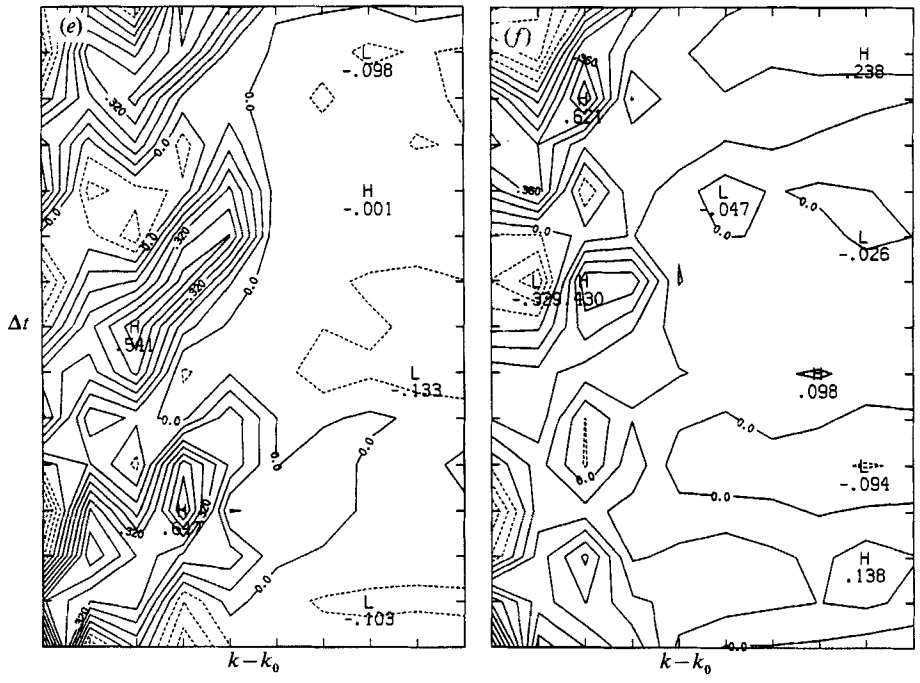

FIGURE 10(*e*,*f*). For caption see facing page.

$$\frac{\langle \Delta\epsilon(k_0, t_0)\,\Delta\epsilon(k_1, t_0+\Delta t)\rangle}{\langle(\Delta\epsilon(k_0, t))^2\rangle^{\frac{1}{2}}\langle(\Delta\epsilon(k_1, t))^2\rangle^{\frac{1}{2}}}$$

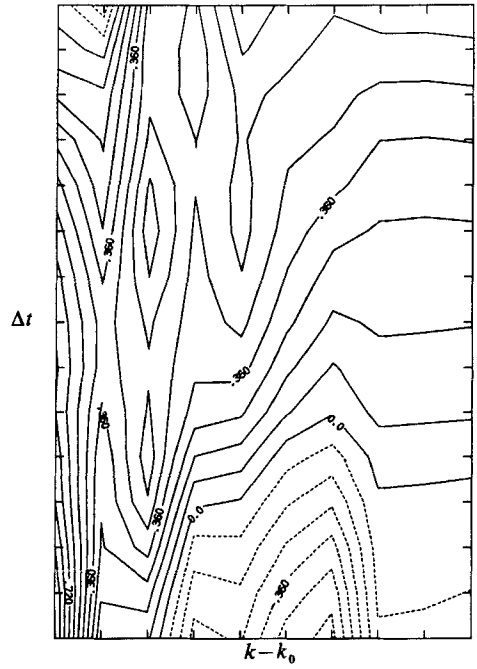

FIGURE 11. Contour plot of time-averaged correlations between three-dimensional dissipation spectra for $k_0 = 4$ and k_1 for time separations Δt from simulation F25. The sample is from $t = 1.15$ to 3.2 and Δt is from 0 to 0.7. Times should be compared to the eddy-turnover time $t_e = 0.85$. Solid lines are positive contours and dashed lines are negative contours.

variable, and observed pulses of energy cascading to high wavenumbers, then dissipating. But there are some significant differences between their model and the Navier–Stokes equation, in addition to the severe wavenumber truncation. They found a third-order quantity that is non-zero, is conserved by the nonlinear terms, and serves as a Hamiltonian for their equations. The closest analogue to this term in the Navier–Stokes equation is the energy-transfer spectrum because it is also third order and because of similarities between the envelopes of the pulses of the Hamiltonian spectrum in Kerr & Siggia (1978) and the envelopes of the pulses in the energy-transfer spectra seen in figures 9 and 10. But the analogy falls short because the energy transfer is not a Hamiltonian and its integral is zero. The helicity is similar to the third-order Hamiltonian of Kerr & Siggia (1978) in that it is an invariant of the nonlinear term of the three-dimensional Navier–Stokes equation that is not positive definite, but the helicity is not a good analogue because it is quadratic. Kerr & Siggia (1978) showed that their model could be derived from a truncated form of Burgers' equation, a one-dimensional equation that is known to form shocks, and the pulses of Kerr & Siggia (1978) were identified with these shocks. Shocks do not exist in an incompressible flow, but this does suggest that the pulses seen here might be identified with the development of sharp structures in the velocity or vorticity field.

The appearance of extended vortex structures in the graphics of Kerr (1985*a*) and Ashurst *et al.* (1987) might represent this process. Lundgren (1982) has a model for anisotropic dissipation structures that is based upon strained vortex tubes similar to those observed by Kerr (1985*a*). This model develops a $k^{-\frac{5}{3}}$ spectrum without corrections when fluctuation pulses are averaged in time, even though the model is anisotropic and the pulses can be intermittent. A crude $k^{-\frac{5}{3}}$ spectrum also occurs in this simulation along with large temporal and spatial intermittency, although large intermittency suggests that corrections to the $-\frac{5}{3}$ law of the type predicted by Kolmogorov (1962) and Frisch *et al.* (1978) would be expected if higher Reynolds numbers could be simulated. However, because those theories neglect temporal intermittency, which this simulation demonstrates is very strong, it is possible that intermittency can be consistent with a $k^{-\frac{5}{3}}$ inertial regime with no corrections in the manner Lundgren (1982) predicts.

While the model of Lundgren (1982) qualitatively resembles the structures of Kerr (1985*a*), Kerr (1987) shows that the most intense vortex stretching and enstrophy production is not associated with intense vorticity, but with regions where sheet-like structures are forming. In addition, Pumir & Kerr (1987) found that oppositely directed vortex filaments develop into vortex sheets whose separation goes to zero through a self-induction process, and Siggia (1984) has shown that anti-parallel pairing is a general property of three-dimensional vortex filaments. In figure 12 the enstrophy-production spectra for the three times discussed by Pumir & Kerr show that the positive peak of these spectra moves to higher wavenumbers with time; a behaviour consistent with figures 9 and 10 and a clear indication of non-local transfer. Together with recent work by Kerr & Hussian (1989) that suggests that in the limit of zero viscosity the vortex sheets of Pumir & Kerr develop a singularity in a convective timescale, the similarities between the transfer spectra of figures 9 and 12 lead to the suggestion that this simple vortex interaction could be a driving mechanism behind the turbulent energy cascade.

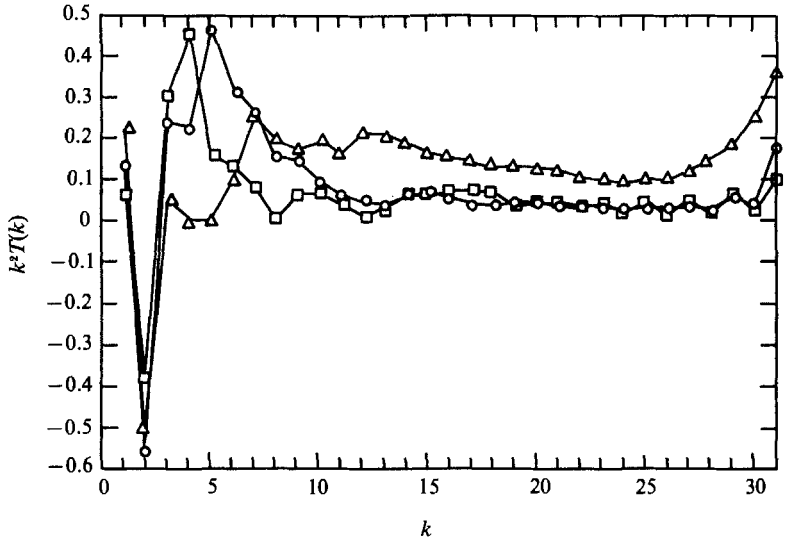

FIGURE 12. Three-dimensional enstrophy-production spectra for discrete times for simulation of oppositely directed vortex sheets discussed by Pumir & Kerr (1987). □, $t = 4$; ○, $t = 5$; △, $t = 6$. Note how the positive peak moves to higher wavenumbers with time.

6. Conclusion

Spectra produced by numerical simulation of the incompressible Navier–Stokes equations and passive-scalar transport equations for a range of Reynolds numbers and Prandtl numbers have been studied in detail. With the qualification that an artificial forcing was used to maintain a statistically steady state, we believe that this is the first time a Kolmogorov inertial subrange has been simulated directly for an extensive period, despite being limited by the mesh size to moderate Reynolds numbers. In other cases where a Kolmogorov spectrum has been found either subgrid modelling was used (Siggia & Patterson 1978) or the spectrum was transient (Brachet *et al.* 1983). That the $-\frac{5}{3}$ regime of Brachet *et al.* (1983) is extensive in wavenumber and that it occurs in a burst, possibly similar to the pulses discussed here, appears likely, but they obtain a Kolmogorov constant that is implausibly large ($\alpha = 4.0$). To show that a spectrum has a valid Kolmogorov regime it should be shown, as in figure 2, that Kolmogorov similarity consistent with experiments is obeyed, even if direct comparisons with experiments are not possible.

The Kolmogorov constant that is found here is also too large, but is consistent with experimental trends at low Reynolds number and there is good agreement between the simulations and the low Reynolds number experiments in the dissipation regime. Based on this success, it is argued that that this simulation can be used to investigate several scalar-variance spectral regimes that are difficult to study experimentally. For $\sigma = 1.0$ the simulations are shown to be consistent with the experimental observation of a k^{-1} regime beginning at lower Prandtl numbers than expected. At low Prandtl numbers, while there is no solid evidence from these calculations as to whether the Batchelor *et al.* (1959) or the Gibson (1968*b*) theory for the spectral form at small Prandtl numbers is correct, two secondary predictions based on Gibson (1968*a*, *b*) are supported; the mixed-derivative skewness is constant and the scalar-dissipation spectra obey Batchelor scaling.

Pulses are observed in the energy-transfer spectrum that have a profile similar to

those observed in the cascade model of Kerr & Siggia (1978). The pulses propagate linearly in time to high wavenumbers and are distinct until the dissipation regime. This would suggest that large-scale intermittency is felt at the smallest scales, which is consistent with the vortex structures found in the graphics of Kerr (1985*a*) and Ashurst *et al.* (1987). A physical-space structure that might be associated with the pulses has been identified by Pumir & Kerr (1987), where similar structures in the enstrophy-production spectra are produced by oppositely directed vortex sheets.

The simulations that produced the spectra discussed here were the largest possible on present computers without extraordinary resources. Despite the limitations, satisfactory comparisons with experiments were obtained and some new insight was gained. As computer speed and memory increases, these results could be extended to higher Reynolds numbers and a wider range of Prandtl numbers, and eventually it would be unnecessary to use an artificial forcing to reach these Reynolds numbers.

I wish to thank C. H. Gibson, R. S. Rogallo, A. Pouquet, and J. Herring for useful discussions. Computational support from NASA Ames Research Center is acknowledged. This work was completed under ARO MIPR No. 129-87.

REFERENCES

Ashurst, W. T., Kerstein, A. R., Kerr, R. M. & Gibson, C. H. 1987 Alignment of vorticity and scalar gradient with strain rate in simulated Navier–Stokes turbulence. *Phys. Fluids* **30**, 2343–2353.

Batchelor, G. K. 1959 Small-scale variation of convected quantities like temperature in turbulent fluid. Part 1. General discussion and the case of small conductivity. *J. Fluid Mech.* **5**, 113–133.

Batchelor, G. K. 1971 *The Theory of Homogeneous Turbulence* (2nd edn.). Cambridge University Press.

Batchelor, G. K., Howells, I. D. & Townsend, A. A. 1959 Small-scale variation of convected quantities like temperature in turbulent fluid. Part 2. The case of large conductivity. *J. Fluid Mech.* **5**, 134–139.

Brachet, M. E., Meiron, D. I., Orszag, S. A., Nickel, B. G., Morf, R. H. & Frisch, U. 1983 Small-scale structure of the Taylor–Green vortex. *J. Fluid Mech.* **130**, 411–452.

Champagne, F. H. 1978 The fine-scale structure of the turbulent velocity field. *J. Fluid Mech.* **86**, 67–108.

Champagne, F. H., Friehe, C. A., LaRue, J. C. & Wyngaard, J. C. 1977 Flux measurements, flux estimation techniques and fine-scale turbulence measurements in the unstable surface layer over land. *J. Atmos. Sci.* **34**, 515.

Chapman, D. R. 1979 Computational aerodynamics development and outlook. *AIAAJ.* **17**, 1293–1313.

Chasnov, J., Canuto, V. M. & Rogallo, R. S. 1988 Turbulence spectrum of a passive temperature field: Results of a numerical simulation. *Phys. Fluids* **31**, 2065–2067.

Clay, J. P. 1973 Turbulent mixing of temperature in water, air and mercury. Ph.D. thesis, University of California at San Diego.

Corrsin, S. 1951 On the spectrum of isotropic temperature fluctuations in isotropic turbulence. *J. Appl. Phys.* **22**, 469–473.

Frisch, U. & Morf, R. 1981 Intermittency and nonlinear dynamics at complex times. *Phys. Rev.* A **23**, 2673.

Frisch, U., Sulem, P. L. & Nelkin, M. 1978 A simple model of intermittent fully developed turbulence. *J. Fluid Mech.* **87**, 719–736.

Gibson, C. H. 1968*a* Fine structure of scalar fields mixed by turbulence. I. Zero-gradient points and minimal-gradient surfaces. *Phys. Fluids* **11**, 2316–2327.

Gibson, C. H. 1968*b* Fine structure of scalar fields mixed by turbulence. II. Spectral theory. *Phys. Fluids* **11**, 2316–2327.

GIBSON, C. H., ASHURST, W. T. & KERSTEIN, A. R. 1988 Mixing of strongly diffusive passive scalars like temperature by turbulence. *J. Fluid Mech.* **194**, 261–293.

GIBSON, C. H. & KERR, R. M. 1987 Evidence of turbulent mixing by the rate-of-strain. Preprint.

HERRING, J. R. & KRAICHNAN, R. H. 1979 A numerical comparison of velocity-based and strain-based Lagrangian-history turbulence approximations. *J. Fluid Mech.* **89**, 581–597.

HERRING, J. R., SCHERTZER, D., LESIEUR, M., NEWMAN, G. R., CHOLLET, J. P. & LARCHEVEQUE, M. 1982 A comparative assessment of spectral closures as applied to passive scalar diffusion. *J. Fluid Mech.* **124**, 411–437.

HILL, R. J. 1978 Models of the scalar spectrum for turbulent advection. *J. Fluid Mech.* **88**, 541–562.

KERR, R. M. 1985*a* Higher-order derivative correlations and the alignment of small-scale structures in isotropic numerical turbulence. *J. Fluid Mech.* **153**, 31–58. (See also *NASA TM* 84407, 1983.)

KERR, R. M. 1985*b* Kolmogorov and scalar-spectral regimes in numerical turbulence. *NASA Tech. Memo* 86699.

KERR, R. M. 1987 Histograms of helicity and strain in numerical turbulence. *Phys. Rev. Lett.* **59**, 783.

KERR, R. M. & HUSSAIN, F. 1989 Simulation of vortex reconnection. *Physica* D **37**, 474–484.

KERR, R. M. & SIGGIA, E. D. 1978 Cascade mode of fully developed turbulence. *J. Statist. Phys.* **19**, 543–552.

KIDA, S. & MURAKAMI, Y. 1987 Kolmogorov similarity in freely decaying turbulence. *Phys. Fluids* **30**, 2030–2039.

KOLMOGOROV, A. N. 1941 Local structure of turbulence in an incompressible fluid at very high Reynolds numbers. *C. R. Acad. Sci. URSS* **30**, 301–305.

KOLMOGOROV, A. N. 1962 A refinement of previous hypotheses concerning the local structure of turbulence in a viscous incompressible fluid at high Reynolds number. *J. Fluid Mech.* **13**, 82–85.

KRAICHNAN, R. H. 1959 The structure of isotropic turbulence at very high Reynolds numbers. *J. Fluid Mech.* **5**, 497–543.

KRAICHNAN, R. H. 1968 Small-scale structure of a scalar field convected by turbulence. *Phys. Fluids* **11**, 945–953.

KRAICHNAN, R. H. 1976 Eddy viscosity in two and three dimensions. *J. Atmos. Sci.* **33**, 1521–1536.

KRAICHNAN, R. H. 1987 Kolmogorov's constant and local interactions. *Phys. Fluids* **30**, 1583–1585.

LUMLEY, J. L. 1965 Interpretation of time spectra measured by high-intensity shear flows. *Phys. Fluids* **8**, 1056–1062.

LUNDGREN, T. S. 1982 Strained spiral vortex model for turbulent fine structure. *Phys. Fluids* **25**, 2193–2203.

MESTAYER, P., CHOLLET, J. P. & LESIEUR, M. 1983 Inertial subrange anomalies of the velocity and scalar variance spectra in three-dimensional turbulence. Preprint.

MONIN, A. S. & YAGLOM, A. M. 1975 *Statistical Fluid Mechanics*, vol. 2. Massachusetts Institute of Technology Press.

OBOUKOV, A. M. 1949 Structure of the temperature field in a turbulent flow. *Izv. Akad. Nauk. SSSR, Geogr. i Geofiz.* **13**, 58–69.

ORSZAG, S. A. 1970 Analytical theories of turbulence. *J. Fluid Mech.* **41**, 363–386.

PAO, Y.-H. 1965 Structure of turbulent velocity and scalar fields at large wavenumbers. *Phys. Fluids* **8**, 1063–1075.

PUMIR, A. & KERR, R. M. 1987 Numerical simulation of interacting vortex tubes. *Phys. Rev. Lett.* **58**, 1636–1639.

SIGGIA, E. D. 1978 Model of intermittency in three-dimensional turbulence. *Phys. Rev.* A **17**, 1166–1176.

SIGGIA, E. D. 1984 Collapse and amplification of a vortex filament. *Phys. Fluids* **28**, 794.

SIGGIA, E. D. & PATTERSON, G. S. 1978 Intermittency effects in a numerical simulation of stationary three-dimensional turbulence. *J. Fluid Mech.* **86**, 567–592.

SREENIVASAN, K. R. 1985 On the fine-scale intermittency of turbulence. *J. Fluid Mech.* **151**, 81.

VAN ATTA, C. W. 1979 Bispectral measurements in turbulence computations. In *Proc. 6th Int. Conf. on Numerical Methods in Fluid Mechanics*. Lecture Notes in Physics, vol. 90 (ed. H. Cabanner, M. Bilt, V. Russnov), pp. 530–536. Springer.

VON NEUMAN, J. 1949 Recent theories of turbulence (A report to Office of Naval Research). In *Collected Works*, vol. 6 (1949–1963), p. 437.

WYNGAARD, J. C. & TENNEKES, H. 1970 Measurements of the small-scale structure of turbulence at moderate Reynolds numbers. *Phys. Fluids* **13**, 1962–1969.

YAKHOT, V. & ORSZAG, S. 1986 Renormalization group analysis of turbulence. I. Basic Theory. *J. Sci. Comput.* **1**, 3.